Proceedings of the ASME 2010 3rd Joint US-European Fluids Engineering Summer Meeting and 8th International Conference on Nanochannels, Microchannels, and Minichannels
FEDSM-ICNMM2010
August 1-5, 2010, Montreal, Canada

FEDSM-ICNMM2010-30084

DYNAMICS OF A FLUID-CONVEYING CANTILEVERED PIPE WITH INTERMEDIATE SPRING SUPPORT

Mergen H. Ghayesh
Department of Mechanical Engineering
McGill University
Montréal, Québec, Canada
Email:mergen.hajghayesh@mail.mcgill.ca

Michael P. Païdoussis
Department of Mechanical Engineering
McGill University
Montréal, Québec, Canada
Email: michael.paidoussis@mcgill.ca

ABSTRACT

The aim of this study is to investigate the three-dimensional (3-D) nonlinear dynamics of a fluid-conveying cantilevered pipe, additionally supported by an array of four springs attached at a point along its length. In the theoretical analysis, the 3-D equations are discretized via Galerkin's technique, yielding a set of coupled nonlinear differential equations. These equations are solved numerically using a finite difference technique along with the Newton-Raphson method. The dynamic behaviour of the system is presented in the form of bifurcation diagrams, along with phase-plane plots, time-histories, PSD plots, and Poincaré maps for two different spring locations and inter-spring configurations. Interesting dynamical phenomena, such as planar or circular flutter, divergence, quasiperiodic and chaotic motions, have been observed with increasing flow velocity. Experiments were conducted for the cases studied theoretically, and good qualitative and quantitative agreement was observed.

1. INTRODUCTION

Fluid-conveying pipes may be found in many engineering systems, e. g. in heat exchangers, power generating plants, fuel pipes in high duty engines, hydropower systems, and solution mining applications. The dynamical behaviour of fluid-conveying pipes additionally supported by an intermediate spring has been studied extensively via linear and nonlinear mathematical models; refer to Païdoussis [1] for a review.

The system of a fluid-conveying pipe can be modelled via linear [2-5] or nonlinear [6-10] theory. Post-critical bifurcations, after the system has lost stability, can only be reliably predicted via nonlinear theory. Also, three-dimensional motions are inherently nonlinear [7, 9]. Therefore, the use of a nonlinear theoretical model is essential.

Early studies focused on the planar motions of the system [1-4, 11-18]; however, with the advent of 3-D models in the 1970s and 80s [6-8] this assumption has become no longer necessary or desirable.

The 3-D dynamics of a fluid-conveying cantilevered pipe, additionally supported by arrays of four springs was investigated by Steindl and Troger [19-21]. In these studies, the system with perfect and broken symmetries was considered and some interesting analytical work was conducted via the centre manifold reduction method and consequently stability boundaries were constructed.

More recently, Païdoussis et al. [10] studied the 3-D dynamics of a fluid-conveying cantilevered pipe with intermediate spring-supports, both theoretically and experimentally. In the theoretical part of this study, the nonlinear equations of motion, newly derived by Wadham-Gagnon et al. [9] were used and it was shown that the system displays diversity of rich dynamical behaviour, depending on the location of the additional support and the inter-spring configuration. These results were confirmed by some experiments.

In this paper, the 3-D dynamics of a fluid-conveying cantilevered pipe additionally supported by a four-spring array is investigated using the 3-D nonlinear equations of motion derived in [9]. Attention is focused in particular on the role of the spring configuration and its location along the pipe length on the post-critical dynamics of the system. Specifically, the dynamics of the system is presented in the form of bifurcation diagrams, time-histories, phase-plane portraits, PSD plots and Poincaré maps for two inter-spring configurations and spring-support locations.

2. PROBLEM STATEMENT, EQUATIONS OF MOTION, AND METHOD OF SOLUTION

A schematic representation of the system considered is shown in Fig.1. This system consists of a pipe of length L, inner/outer diameter D_i /D_o, flexural rigidity EI, density ρ_p, mass per unit length m, conveying fluid of density ρ_f, mass per unit length M, with flow velocity U. An array of four springs of individual stiffness k is attached at a distance L_s from the fixed end of the pipe.

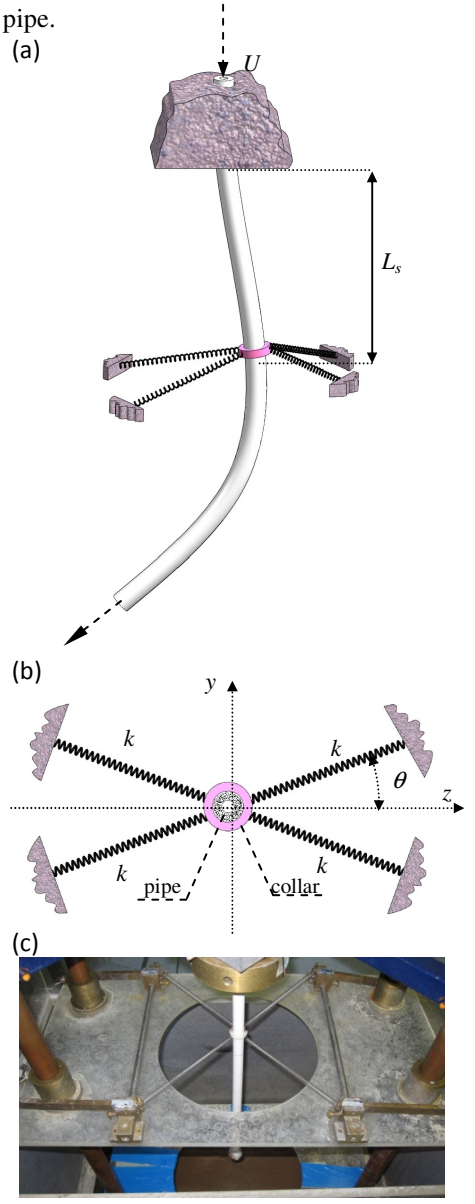

Figure1. Schematic representation of a fluid-conveying cantilevered pipe with added "intermediate" support by an array of springs at $x = L_s$: (a) deformed system; (b) top view showing the four-spring configuration; (c) experimental set-up.

The equation of motion for a cantilevered pipe with intermediate spring support at L_s is given in Appendix A. Some of the dimensionless parameters in the equations of motion, repeated here for convenience, are:

$$u = \left(\frac{M}{EI}\right)^{1/2} UL,\ \gamma = \frac{m+M}{EI} L^3 g,\ \beta = \frac{M}{m+M}, \qquad (1)$$

where u is the dimensionless flow velocity, γ a dimensionless gravity parameter, and β a mass parameter.

The dimensionless set of nonlinear partial differential equations (Appendix A) is discretized using Galerkin's scheme with the plain cantilever-beam eigenfunctions as the basis functions (Appendix B). The resultant set of ordinary differential equations is then solved using Houbolt's finite difference scheme, yielding the static displacements or the amplitudes of oscillation as functions of time. From these time-histories, the modal and spectral characteristics of the flow-induced motions can be obtained and bifurcation diagrams may be constructed, using u as the bifurcation parameter. Furthermore, the trigger used for the Poincaré map was that $d\zeta(1,\tau)/d\tau$=0, i.e. when the ζ-component of the velocity crosses zero.

In the calculations, the following common parameters have been used: L=0.443 m, D_i /D_o=6.4/15.7 mm, EI=7.42 × 10^{-3} N·m^2, ρ_p=1167 kg/m^3, ρ_f=999 kg/m^3, m=0.189 kg/m, M=0.0320 kg/m, L_o=0.0635 m, k=17.63 N/m; γ=25.3, and β= 0.145, corresponding to the experimental system described in Section 4; L_o is defined in Appendix A . On the other hand, L_s, θ and R_o were varied.

The bifurcation diagrams have been obtained by employing increments of 0.2 in the flow velocity u.

3. THEORETICAL RESULTS

In this section, the dynamics of the system for two inter-spring configurations and spring-support locations is studied theoretically.

3.1. Dynamics of the system with L_s=0.2L and θ=45^o

For this case, the four springs are located at L_s=0.2L, near the clamped end of the pipe, at 45^o to each other (see Fig. 1). The overall dynamical behaviour of the system is summarized in the bifurcation diagram of Fig.2, showing the dimensionless maximum/minimum free-end displacements η and ζ, respectively in the y and z directions, versus the dimensionless flow velocity u.

A supercritical Hopf bifurcation occurs at u=6.8, leading to a planar limit-cycle motion, slanted relative to the y and z axes. Figure 3 shows (a) the time histories, (b) the pipe-tip motion (i.e. motion of the free end of the pipe) in a plane perpendicular to the pipe, and (c) the phase-plane diagram for the η motion. The frequency of oscillation (in cycles per dimensionless seconds) is f=3.08.

With increasing u, the following major bifurcations occur.

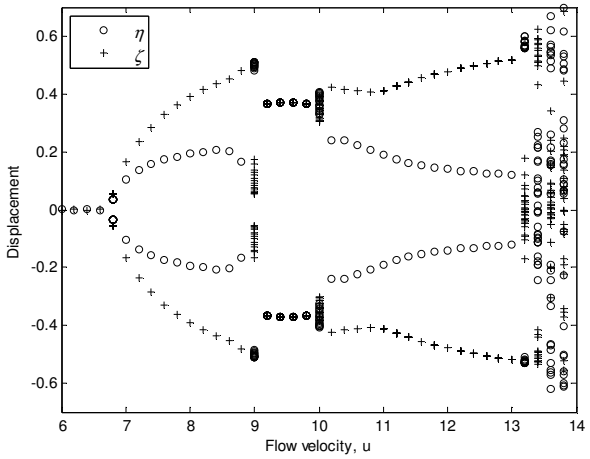

Figure 2. Bifurcation diagram for the pipe with L_s=0.2L and θ=45°, showing minimum/maximum values of the tip (free-end) displacement in the η and ζ directions.

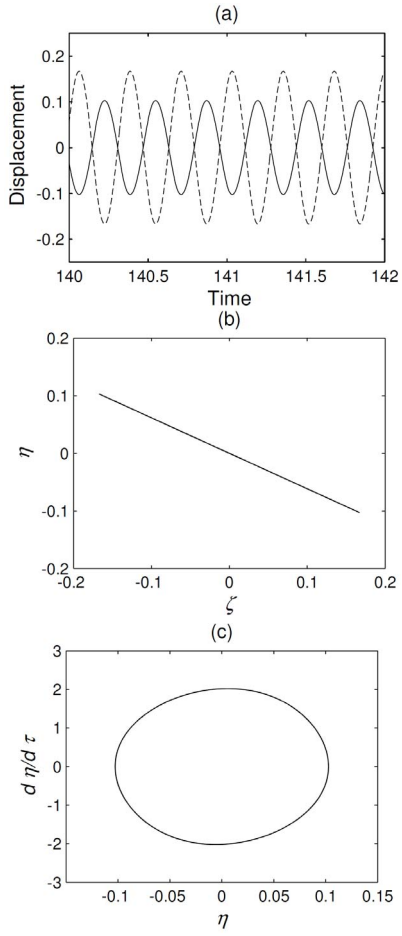

Figure 3. Planar flutter at a dimensionless flow velocity of u=7.0: (a) time trace of η (solid line) and ζ (dashed line); (b) top view of the tip displacement of the pipe; (c) phase-plane portrait.

(i) At u=9.0, quasiperiodic and three-dimensional (3-D) oscillations occur, as shown in Fig.4. As seen in Fig.4 (b), the power spectral density (PSD), obtained via a Fast Fourier Transform of the time trace, yields the two fundamental frequencies f_1= 3.84 and f_2= 11.05, arbitrarily selected as the first two and largest frequencies in the spectrum (f_3=2f_2-f_1 and f_4=3f_2-2f_1 *et seq.*).

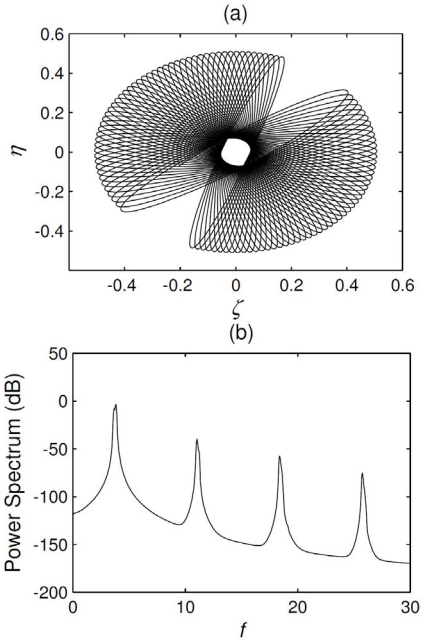

Figure 4. Quasiperiodic motion at u=9.0: (a) top view of the tip displacement of the pipe; (b) PSD plot, showing the dimensionless fundamental frequencies of f_1= 3.84 and f_2= 11.05.

(ii) The above-mentioned 3-D quasiperiodic motion changes to periodic motion once more at u=9.2, involving equal amplitudes in η and ζ directions, but now a circular one. Therefore, the quasiperiodicity in Fig.4 at u=9.0 appears to be a bridge between the planar (6.8≤u≤8.8) and the 3-D circular (9.2≤u≤9.8) periodic motions.

(iii) A small quasiperiodic window occurs once again in the vicinity of u=10 (f_1= 4.39 and f_2=13.31; f_3=2 f_2- f_1 and f_4=3 f_2-2 f_1 *et seq.*).

(iv) The motion becomes periodic once again at u=10.2, but planar and with unequal η and ζ amplitudes.

(v) The 3-D motion becomes quasiperiodic yet again at u=13.2, as shown in Fig.5; here f_1=2.35 and f_2=3.54, with f_3=6f_2-3f_1 and f_4=7 f_2-3f_1.

(vi) As the flow velocity is increased further, the oscillation becomes chaotic at u=13.6, as illustrated in the tip motion of Fig. 6 (a), the Poincaré map of Fig. 6(b), and PSD of Fig. 6(c).

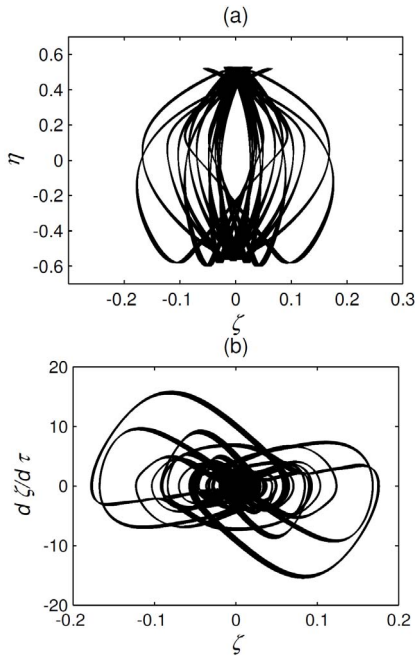

Figure 5. 3-D quasiperiodic motion at u=13.2: (a) top view of the tip displacement of the pipe; (b) phase-plane portrait of ζ motion.

3.2. Dynamics of the system with L_s=0.7L and θ=0^o

In this case, the array of four springs is positioned considerably closer to the free end and all four springs are in the same plane, along the z-axis. In this case stability is lost by a static divergence (buckling) at u=7.8 in the plane of highest resistance (z direction) against the springs (Fig. 7).

(i) As the flow velocity is increased, the amplitude of buckling increases, as shown in Fig. 7.

(ii) This non-zero static solution becomes unstable via a Hopf bifurcation at u=8.6, leading to planar flutter in the ζ direction around the initial non-zero fixed point. This motion lasts till u=9.0 (Fig.8(a)).

(iii) At u=9.2, the 2-D periodic motion soon becomes quasiperiodic, as shown in Fig. 8 (b), and this lasts till u=9.8. The top view of the tip displacement for flow velocities of u=9.4, u=9.6 are shown in Figs.8(c) and (d), respectively.

(iv) As u is increased further, a 3-D periodic motion occurs at u=10.0.

(v) There is a return to a quasiperiodic motion at u=10.2.

(vi) As u is increased a little further, the pipe returns to a periodic oscillation at u=10.4, characterized by an amplitude jump. Before this jump (u≤10.2), the pipe undergoes mainly a combination of first and second beam-mode travelling-wave components, whereas after the amplitude jump (u>10.2), the third mode becomes dominant.

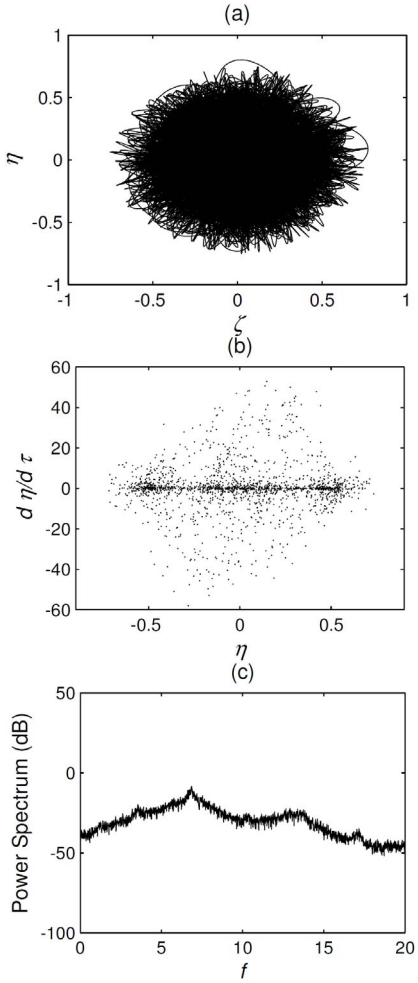

Figure 6. 3-D chaotic motion at u=13.6: (a) tip displacement of the pipe; (b) Poincaré map; (c) PSD plot.

4. EXPERIMENTS

4.1. Apparatus, procedure and data recorded

The experiments were conducted with a silicone rubber pipe with the geometrical and physical characteristics corresponding to the theoretical values of Section 2. The experimental apparatus is similar to that utilized by Païdoussis et al. [10], and its detailed description can be found therein.

The flow rate is measured using an Omega DPF64 ratemeter and an Omega FMG710 flowmeter. The displacement of a point along the pipe length is recorded with a non-contacting optical tracking system (Optron 806-50-X) and Welch's method is implemented in MATLAB for FFT analysis of this signal. These

FFTs serve as a good discriminant for periodic, quasiperiodic and chaotic motions.

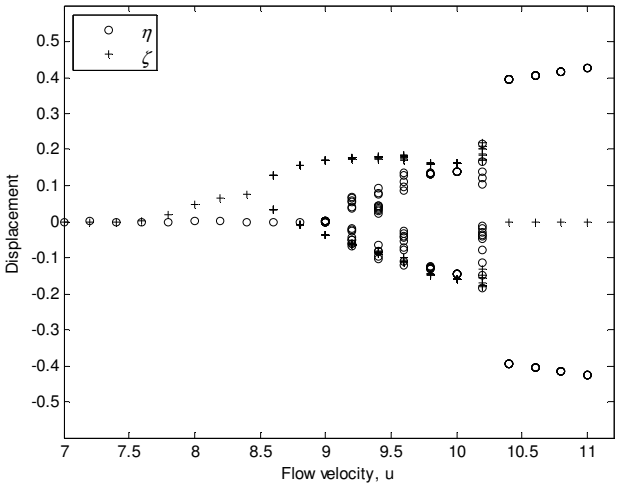

Figure 7. Bifurcation diagram for the pipe with L_s=0.7L and θ=0°, showing minimum/maximum values of tip displacement in η and ζ directions.

The maximum flow velocity attainable is u≈11.8; hence comparison with theory cannot be made beyond this value.

The experimental results as well as their theoretical counterparts are given in the form of tables of u and f for the various bifurcation points. The values of dimensionless flow velocities and frequencies are accurate to within ±0.05.

4.2. Results for the system with L_s=0.2L and θ=45°

For this case, planar flutter occurred at u=6.7 with a frequency of f=3.3. As the flow rate was increased further, the oscillation became quasiperiodic at u=9.1 with the fundamental frequencies f_1=4.1 and f_2=8.2 (f_3=2f_2-f_1 and f_4=3f_2-2f_1 *et seq.*). A small increase in the flow rate caused the system to switch to 3-D circular motion at u=9.3 with f=4.3. At higher flow velocity, the system resumes planar oscillation at u=10.1 with f=4.6.

As seen in Table1, the experimental results for this case are in good qualitative and quantitative agreement with the theoretical results obtained in Section 3.1, except for the second, very narrow, quasiperiodic window predicted to take place at u=10.0 by the theory, but never observed in the experiments.

4.3. Results for the system with L_s=0.7L and θ=0°

For this system, the first instability was divergence in the η direction at u=7.6. The amplitude of divergence grew as the flow velocity was increased, and at u=8.8 small oscillations were superimposed on the buckled state in the ζ direction, i.e. in the plane perpendicular to the initial plane of buckling, with a frequency of f=8.0. As the flow velocity was increased further, the onset of quasiperiodic motion occurred at u=9.1 with fundamental frequencies f_1=8.1 and f_2=16.7 (f_3=f_1+f_2). This motion lasted till u=10.0, with f_1=7.4 and f_2=16.0, still with f_3=f_1+f_2; it then became a 2-D planar periodic pure η motion at u=10.3 (f=6.9), as seen in Table 2.

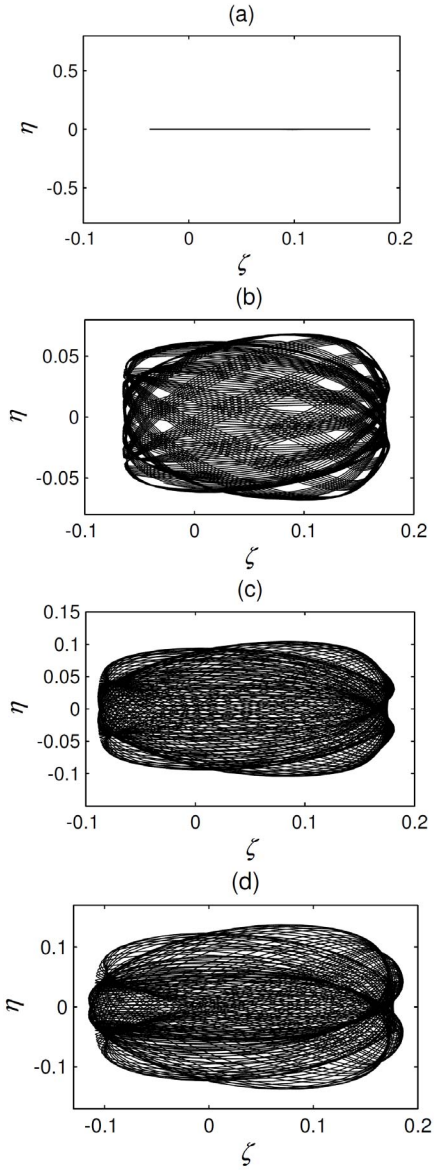

Figure 8. (a)-(d) Top view of the tip displacement of the pipe at (a) u=9.0, (b) u=9.2, (c) u=9.4, and (d) u=9.6, respectively.

It is seen in Table 2 that the experimental observations are in quantitative agreement with the theoretical results. They are also in agreement qualitatively, except for the interval of divergence for 7.6<u<8.8, where the buckling occurred in the plane of *least* resistance (η direction), as opposed to the theoretical results.

5. CONCLUSIONS

The 3-D dynamical behaviour of a fluid-conveying cantilevered pipe with intermediate four-spring support has been studied in this paper. Changing spring locations and inter-spring configurations, two cases displaying the most interesting dynamical behaviour have been presented. The theoretical results were confirmed by conducting some experiments.

The system displays very rich 3-D dynamics by varying the dimensionless flow velocity, spring-support location and inter-spring configuration. This includes planar or orbital motions, quasiperiodic motions followed by either periodic oscillations or chaotic motions (either 2-D or 3-D).

Generally, there is very good agreement between theoretical and experimental results. There are two points of disagreement: (i) for the system with L_s=0.2L and θ=45^o, a quasiperiodic motion occurs according to theory in a small interval of u around u=10.0, but has never been observed in the experiment; (ii) for the system with L_s=0.7L and θ=0^o, a divergence is predicted by theory to occur in the plane of highest resistance, i.e. in the ζ direction, while in the experiments the buckling develops in the η direction (in the plane of least resistance). No definite reason has been determined for this discrepancy, but the influence of imperfections is suspected.

In conclusion, it can be said that adding an intermediate spring support to a fluid-conveying pipe enriches the dynamics of the system substantially, specifically by revealing the existence of quasiperiodic and chaotic oscillations, which have never been observed for a plain pipe (i.e., a pipe without additional masses or springs attached to it). All the results presented in this paper are for constant values of γ, β and k. It would be interesting to expand this study by varying these parameters also.

Table 1
Flow velocities and frequencies of *bifurcation points* for the system with L_s=0.2L and θ=45^o:
Theory versus experiment

	Values of u		Values of f[1]	
	Theory	Experiment	Theory	Experiment
Planar flutter (Hopf bifurcation)	6.80	6.7	3.13	3.3
First quasiperiodic motion	9.00	9.1	3.84 and 11.05	4.1 and 8.2
First circular motion	9.20	9.3	3.91	4.3
Second quasiperiodic motion	10.0	not observed	4.39 and 13.31	not observed
First planar oscillation after the second quasiperiodic motion	10.2	10.1	4.69	4.6

Table 2
Flow velocities and frequencies of *bifurcation points* for the system with L_s=0.7L and θ=0^o:
Theory versus experiment

	Values of u		Values of f	
	Theory	Experiment	Theory	Experiment
Divergence	7.8[2]	7.6[3]	-	-
Planar flutter in ζ direction around the non-zero fixed point	8.6	8.8	9.37	8.0
Onset of quasiperiodic Motion	9.2	9.1	8.10 and 16.99	8.1 and 16.7
End of quasiperiodic motion	10.2	10.0	8.40 and 17.28	7.4 and 16.0
First planar oscillations in η direction after the last quasiperiodic motion	10.4	10.3	8.10	6.9

ACKNOWLEDGMENTS

The authors would like to thank Dr Christian Semler and Stephanie Rinaldi of McGill University and Yahya Modarres-Sadeghi currently at the University of Massachusetts for their assistance. Financial support from the Natural Sciences and Engineering Research Council (NSERC) of Canada is also gratefully acknowledged, and the first author is also grateful for a MEDA Award accorded to him by McGill University.

REFERENCES

[1] M.P. Païdoussis, 1998. *Fluid–Structure Interactions: Slender Structures and Axial Flow*, *vol. 1*. Academic Press, London, UK.

[1] f is dimensionless frequency (cycles per dimensionless second).

[2] in ζ direction

[3] in η direction

[2] R.W. Gregory and M.P. Païdoussis, 1966. *Proceedings of the Royal Society A* **293**, 512–527. Unstable oscillations of tubular cantilevers conveying fluid-I. Theory.

[3] R.W. Gregory and M.P. Païdoussis, 1966. *Proceedings of the Royal Society A* **293**, 528–542. Unstable oscillations of tubular cantilevers conveying fluid-II. Experiments.

[4] Y. Sugiyama, Y. Tanaka, T. Kishi and H. Kawagoe, 1985. *Journal of Sound and Vibration* **100**, 257-270. Effect of a spring support on the stability of pipes conveying fluid.

[5] M.V. Vassil and P. A. Djondjorov, 2006. *Journal of Sound and Vibration* **297**, 414–419. Dynamic stability of viscoelastic pipes on elastic foundations of variable modulus.

[6] T.S. Lundgren, P.R. Sethna and A.K. Bajaj, 1979. *Journal of Sound and Vibration* **64**, 553–571. Stability boundaries for flow induced motions of tubes with an inclined terminal nozzle.

[7] A.K. Bajaj, P.R. Sethna and T.S. Lundgren, 1980. *SIAM Journal of Applied Mathematics* **39**, 213–230. Hopf bifurcation phenomena in tubes carrying fluid.

[8] J. Rousselet and G. Hermann, 1981. *Journal of Applied Mechanics* **48**, 943–947. Dynamic behaviour of continuous cantilevered pipes conveying fluid near critical velocities.

[9] M. Wadham-Gagnon, M.P. Païdoussis and C. Semler, 2007. *Journal of Fluids and Structures* **23**, 545–567. Dynamics of cantilevered pipes conveying fluid. Part 1: Nonlinear equations of three-dimensional motion.

[10] M.P. Païdoussis, C. Semler and M. Wadham-Gagnon, 2007. *Journal of Fluids and Structures* **23**, 569–587. Dynamics of cantilevered pipes conveying fluid. Part 2: dynamics of the system with intermediate spring support.

[11] F.-J. Bourrières, 1939. *Publications Scientifiques et Techniques du Ministère de l'Air*, **147**. Sur un phénomène d'oscillation auto-entretenue en mécanique des fluides réels.

[12] T.B. Benjamin, 1961. *Proceedings of the Royal Society of London Series A* **261**, 457–486. Dynamics of a system of articulated pipes conveying fluid: I. Theory.

[13] T.B. Benjamin, 1961. *Proceedings of the Royal Society of London Series A* **261**, 487–499. Dynamics of a system of articulated pipes conveying fluid: II. Experiment.

[14] M.P. Païdoussis, 1970. *Journal of Mechanical Engineering Science* **12**, 85–103. Dynamics of tubular cantilevers conveying fluid.

[15] K. Jendrzejczyk and S.S. Chen, 1985. *Thin-Walled Structures* **3**, 109–134. Experiments on tubes conveying fluid.

[16] D. M. Tang and E. H. Dowell, 1988. *Journal of Fluids and Structures* **2**, 263-283. Chaotic oscillations of a cantilevered pipe conveying fluid.

[17] M.P. Païdoussis and F. C. Moon, 1988. *Journal of Fluids and Structures* **2**, 567-591. Nonlinear and chaotic fluidelastic vibrations of a flexible pipe conveying fluid.

[18] M.P. Païdoussis and C. Semler, 1993. *Journal of Fluids and Structures* **7**, 269–298. Nonlinear dynamics of a fluid-conveying cantilevered pipe with an intermediate spring support.

[19] A. Steindl and H. Troger, 1995. *Nonlinear Dynamics* **7**, 165-193. Nonlinear three-dimensional oscillations of elastically constrained fluid conveying viscoelastic tubes with perfect and broken O(2)-symmetry.

[20] A. Steindl and H. Troger, 1995. *Nonlinear Dynamics* **8**, 161-178. One and two-parameter bifurcations to divergence and flutter in the three-dimensional motions of a fluid conveying viscoelastic tube with D4-symmetry.

[21] A. Steindl and H. Troger, 1996. *Applied Mathematics and Computation* **78**, 269-277. Heteroclinic cycles in the three-dimensional postbifurcation motion of O(2)-symmetric fluid conveying tubes.

APPENDIX A

THE EQUATIONS OF MOTION

The set of 3-D nonlinear equations of motion [9] for the fluid-conveying cantilevered pipe with intermediate springs, are given below.

The *y*-equation

$$
\begin{aligned}
&\eta''''+\ddot{\eta}+2u\sqrt{\beta}\dot{\eta}'+u^2\eta''+\gamma\eta' \\
&-\gamma\eta''(1-\xi)+\gamma\left(\tfrac{1}{2}\eta'^3+\tfrac{1}{2}\eta'\zeta'^2\right) \\
&-\gamma\left(\tfrac{3}{2}\eta'^2\eta''+\tfrac{1}{2}\zeta'^2\eta''+\eta'\zeta'\zeta''\right)(1-\xi) \\
&+2u\sqrt{\beta}\left(\eta'^2\dot{\eta}'+\eta'\zeta'\dot{\zeta}'-\eta''\int_\xi^1\left(\eta'\dot{\eta}'+\zeta'\dot{\zeta}'\right)d\xi\right) \\
&+u^2\left(\eta'^2\eta''+\eta'\zeta'\zeta''-\eta''\int_\xi^1\left(\eta'\eta''+\zeta'\zeta''\right)d\xi\right) \\
&+\left(\eta'^2\eta''''+4\eta'\eta''\eta'''+\eta''^3\right. \\
&\left.+\eta'\zeta'\zeta''''+3\eta'\zeta''\zeta'''+\eta''\zeta'\zeta'''+\eta''\zeta''^2\right) \\
&+\eta'\int_0^\xi\left(\dot{\eta}'^2+\eta'\ddot{\eta}'+\dot{\zeta}'^2+\zeta'\ddot{\zeta}'\right)d\xi \\
&-\eta''\int_\xi^1\int_0^\xi\left(\dot{\eta}'^2+\eta'\ddot{\eta}'+\dot{\zeta}'^2+\zeta'\ddot{\zeta}'\right)d\xi d\xi \\
&+\left(\left(\kappa_{yl}\eta+\kappa_{ynl}\eta^3+\kappa_{yz}\eta\zeta^2\right)\right. \\
&\left.+\kappa_x\eta'\int_0^\xi\left(\zeta'^2+\eta'^2\right)d\xi\right)\delta(\xi-\xi_s) \\
&-\kappa_x\eta''\mu(0\to\xi_s)\int_0^{\xi_s}\left(\zeta'^2+\eta'^2\right)d\xi=0;
\end{aligned}
\tag{A.1}
$$

The *z*-equation

$$
\begin{aligned}
&\zeta''''+\ddot{\zeta}+2u\sqrt{\beta}\dot{\zeta}'+u^2\zeta''+\gamma\zeta' \\
&-\gamma\zeta''(1-\xi)+\gamma\left(\tfrac{1}{2}\zeta'^3+\tfrac{1}{2}\zeta'\eta'^2\right) \\
&-\gamma\left(\tfrac{3}{2}\zeta'^2\zeta''+\tfrac{1}{2}\eta'^2\zeta''+\zeta'\eta'\eta''\right)(1-\xi) \\
&+2u\sqrt{\beta}\left(\zeta'^2\dot{\zeta}'+\zeta'\eta'\dot{\eta}'-\zeta''\int_\xi^1\left(\zeta'\dot{\zeta}'+\eta'\dot{\eta}'\right)d\xi\right) \\
&+u^2\left(\zeta'^2\zeta''+\zeta'\eta'\eta''-\zeta''\int_\xi^1\left(\zeta'\zeta''+\eta'\eta''\right)d\xi\right) \\
&+\left(\zeta'^2\zeta''''+4\zeta'\zeta''\zeta'''+\zeta''^3\right. \\
&\left.+\zeta'\eta'\eta''''+3\zeta'\eta''\eta'''+\zeta''\eta'\eta'''+\zeta''\eta''^2\right) \\
&+\zeta'\int_0^\xi\left(\dot{\zeta}'^2+\zeta'\ddot{\zeta}'+\dot{\eta}'^2+\eta'\ddot{\eta}'\right)d\xi \\
&-\zeta''\int_\xi^1\int_0^\xi\left(\dot{\zeta}'^2+\zeta'\ddot{\zeta}'+\dot{\eta}'^2+\eta'\ddot{\eta}'\right)d\xi d\xi \\
&+\left(\left(\kappa_{zl}\zeta+\kappa_{znl}\zeta^3+\kappa_{yz}\zeta\eta^2\right)\right. \\
&\left.+\kappa_x\zeta'\int_0^\xi\left(\zeta'^2+\eta'^2\right)d\xi\right)\delta(\xi-\xi_s) \\
&-\kappa_x\zeta''\mu(0\to\xi_s)\int_0^{\xi_s}\left(\zeta'^2+\eta'^2\right)d\xi=0.
\end{aligned}
\tag{A.2}
$$

In Eqs. (A.1) and (A.2), the following dimensionless quantities have been used:

$$
\begin{aligned}
&\xi=\frac{s}{L},\ \xi_s=\frac{L_s}{L},\ \eta=\frac{v}{L},\ \zeta=\frac{w}{L}, \\
&\tau=\left(\frac{EI}{m+M}\right)^{1/2}\frac{t}{L^2},\ u=\left(\frac{M}{EI}\right)^{1/2}UL, \\
&\gamma=\frac{m+M}{EI}L^3g,\quad \beta=\frac{M}{m+M}, \\
&\kappa_x=\frac{K_xL^3}{EI},\ \kappa_{yl}=\frac{K_{yl}L^3}{EI},\ \kappa_{zl}=\frac{K_{zl}L^3}{EI}, \\
&\kappa_{ynl}=\frac{K_{ynl}L^5}{EI},\ \kappa_{znl}=\frac{K_{znl}L^5}{EI},\ \kappa_{yz}=\frac{K_{yz}L^5}{EI},
\end{aligned}
\tag{A.3}
$$

in which

$$
\begin{aligned}
&K_x=2k\left(1-\frac{L_o}{R_o}\right),\ K_{yl}=4k\left(1-\frac{L_o}{R_o}\cos^2\theta\right), \\
&K_{ynl}=2k\frac{L_o}{R_o^3}\cos^2\theta\left(\cos^2\theta-4\sin^2\theta\right), \\
&K_{yz}=2k\frac{L_o}{R_o^3}\left(15\cos^2\theta\sin^2\theta-2\right), \\
&K_{zl}=4k\left(1-\frac{L_o}{R_o}\sin^2\theta\right),
\end{aligned}
$$

$$K_{znl} = 2k\frac{L_o}{R_o^3}\sin^2\theta\left(\sin^2\theta - 4\cos^2\theta\right),$$

$$K_{yz} = 2k\frac{L_o}{R_o^3}\left(15\cos^2\theta\sin^2\theta - 2\right). \quad \text{(A.4)}$$

In the above equations, ξ is the dimensionless distance along the pipe, ξ_s the dimensionless location of the attachment point of the springs, η the dimensionless transverse displacement in the *v* direction, and ζ in the *w* direction, and τ is dimensionless time; *s* is the distance along the pipe, *L* the pipe length, *v* the displacement in the *y* direction, *w* the displacement in *z* direction, *t* is time, *k* the linear stiffness of each spring, and L_0 and R_0 the unstretched and stretched lengths of the spring; *u* is the dimensionless flow velocity, γ a dimensionless gravity parameter, β a mass parameter; the "*K*"s are constant stiffness coefficients related to the spring array, the subscripts identifying the direction in which they have influence (*x*, *y* or *z*) as well as whether they are associated with linear (*l*) or nonlinear (*nl*) terms; $\mu(0 \to L_s)$ is the Heaviside function, having value of 1 in the interval [0, L_s]and zero elsewhere. Equations (A.1) and (A.2) are correct to $O(\varepsilon^3)$, where η and ζ are of $O(\varepsilon)$.

APPENDIX B

THE DISCRETIZED EQUATIONS OF MOTION

Galerkin's discretization method is applied to the equations of motion, such that

$$\eta(\xi,\tau) = \sum_{r=1}^{N}\phi_r(\xi)\,q_r(\tau) \quad \text{(B.1)}$$

$$\zeta(\xi,\tau) = \sum_{r=1}^{N}\psi_r(\xi)\,p_r(\tau) \quad \text{(B.2)}$$

in which $\phi_r(\xi)$ and $\psi_r(\xi)$ are the dimensionless cantilever beam eigenfunctions, which satisfy the boundary conditions. Once Eqs. (B.1) and (B.2) are substituted into Eqs. (A.1) and (A.2), the resulting equations are multiplied by the corresponding beam eigenfunction and integrated over ξ from 0 to 1, yielding

$$\begin{aligned}
&m_{ij}\ddot{q}_j + c_{ij}\dot{q}_j + \left(k_{ij} + \kappa_{ij}^{ly}\right)q_j + \left(B_{ijkl} + \kappa_{ijkl}^{nly}\right)q_j q_k q_l \\
&+D_{ijkl}\,q_j q_k \dot{q}_l + E_{ijkl}\,q_j \dot{q}_k \dot{q}_l \\
&+F_{ijkl}\,q_j q_k \ddot{q}_l + \left(H_{ijkl} + \kappa_{ijkl}^{yzz}\right)q_j p_k p_l \\
&+L_{ijkl}\,q_j p_k \dot{p}_l + M_{ijkl}\,q_j \dot{p}_k \dot{p}_l + N_{ijkl}\,q_j p_k \ddot{p}_l = 0,
\end{aligned} \quad \text{(B.3)}$$

$$\begin{aligned}
&m_{ij}\ddot{p}_j + c_{ij}\dot{p}_j + \left(k_{ij} + \kappa_{ij}^{lz}\right)p_j + \left(B_{ijkl} + \kappa_{ijkl}^{nlz}\right)p_j p_k p_l \\
&+D_{ijkl}\,p_j p_k \dot{p}_l + E_{ijkl}\,p_j \dot{p}_k \dot{p}_l \\
&+F_{ijkl}\,p_j p_k \ddot{p}_l + \left(H_{ijkl} + \kappa_{ijkl}^{zyy}\right)p_j q_k q_l \\
&+L_{ijkl}\,p_j q_k \dot{q}_l + M_{ijkl}\,p_j \dot{q}_k \dot{q}_l + N_{ijkl}\,p_j q_k \ddot{q}_l = 0.
\end{aligned} \quad \text{(B.4)}$$

where

$$m_{ij} = \int_0^1 \phi_i\phi_j\,d\xi + \Gamma\left[\phi_i\phi_j\right]_{\xi=1}, \quad \text{(B.5)}$$

$$c_{ij} = 2u\sqrt{\beta}\int_0^1 \phi_i\phi_j'\,d\xi, \quad \text{(B.6)}$$

$$\begin{aligned}
k_{ij} &= \int_0^1 \phi_i\phi_j''''\,d\xi + \left(u^2 - \gamma\Gamma\right)\int_0^1 \phi_i\phi_j''\,d\xi \\
&+\gamma\int_0^1 \phi_i\phi_j'\,d\xi + \gamma\Gamma\left[\phi_i\phi_j'\right]_{\xi=1} \\
&-\gamma\left(\int_0^1 \phi_i\phi_j''\,d\xi - \int_0^1 \phi_i\xi\phi_j''\,d\xi\right),
\end{aligned} \quad \text{(B.7)}$$

$$\begin{aligned}
B_{ijkl} &= u^2\int_0^1 \phi_i\left(\phi_j'\phi_k'\phi_l'' - \phi_j''\int_\xi^1 \phi_k'\phi_l''\,d\xi\right)d\xi \\
&+\gamma\int_0^1 \phi_i\left(\tfrac{1}{2}\phi_j'\phi_k'\phi_l' - \tfrac{3}{2}(1-\xi)\phi_j'\phi_k'\phi_l''\right)d\xi \\
&-\gamma\Gamma\left(\int_0^1 \phi_i\left(\tfrac{3}{2}\phi_j'\phi_k'\phi_l''\right)d\xi - \tfrac{1}{2}\left[\phi_i\phi_j'\phi_k'\phi_l'\right]_{\xi=1}\right) \\
&+\int_0^1 \phi_i\left(\phi_j'\phi_k'\phi_l'''' + 4\phi_j'\phi_k''\phi_l''' + \phi_j''\phi_k''\phi_l''\right)d\xi,
\end{aligned} \quad \text{(B.8)}$$

$$D_{ijkl} = 2u\sqrt{\beta}\int_0^1 \phi_i\left(\phi_j'\phi_k'\phi_l' - \phi_j''\int_\xi^1 \phi_k'\phi_l'\,d\xi\right)d\xi, \quad \text{(B.9)}$$

$$\begin{aligned}
E_{ijkl} = F_{ijkl} &= \int_0^1 \phi_i\left(\phi_j'\int_0^\xi \phi_k'\phi_l'\,d\xi - \phi_j''\int_\xi^1\int_0^\xi \phi_k'\phi_l'\,d\xi d\xi\right)d\xi \\
&+\Gamma\left[\phi_i\phi_j'\right]_{\xi=1}\int_0^1 \phi_k'\phi_l'\,d\xi - \Gamma\int_0^1 \phi_i\phi_j''\,d\xi\int_0^1 \phi_k'\phi_l'\,d\xi,
\end{aligned} \quad \text{(B.10)}$$

$$H_{ijkl} = \gamma\int_0^1 \phi_i\left[\tfrac{1}{2}\phi_j'\psi_k'\psi_l' - (1-\xi)\left(\tfrac{1}{2}\phi_j''\psi_k'\psi_l' + \phi_j'\psi_k'\psi_l''\right)\right]d\xi$$
$$-\gamma\Gamma\left(\int_0^1 \phi_i\left(\tfrac{1}{2}\phi_j''\psi_k'\psi_l' + \phi_j'\psi_k'\psi_l''\right)d\xi - \tfrac{1}{2}\left[\phi_i\phi_j'\psi_k'\psi_l'\right]_{\xi=1}\right)$$
$$+u^2\int_0^1 \phi_i\left(\phi_j'\psi_k'\psi_l'' - \phi_j''\int_\xi^1 \psi_k'\psi_l''\,d\xi\right)d\xi \qquad \text{(B.11)}$$
$$+\int_0^1 \phi_i\left(\phi_j'\psi_k'\psi_l'''' + 3\phi_j'\psi_k''\psi_l''' + \phi_j''\psi_k'\psi_l''' + \phi_j''\psi_k''\psi_l''\right)d\xi,$$

$$L_{ijkl} = 2u\sqrt{\beta}\int_0^1 \phi_i\left(\phi_j'\psi_k'\psi_l' - \phi_j''\int_\xi^1 \psi_k'\psi_l'\,d\xi\right)d\xi, \qquad \text{(B.12)}$$

$$M_{ijkl} = N_{ijkl} = \int_0^1 \phi_i\left(\phi_j'\int_0^\xi \psi_k'\psi_l'\,d\xi - \phi_j''\int_\xi^1\int_0^\xi \psi_k'\psi_l'\,d\xi d\xi\right)d\xi$$
$$+\Gamma\left[\phi_i\phi_j'\right]_{\xi=1}\int_0^1 \psi_k'\psi_l'\,d\xi - \Gamma\int_0^1 \phi_i\phi_j''d\xi\int_0^1 \psi_k'\psi_l'\,d\xi; \qquad \text{(B.13)}$$

$$\kappa_{ij}^{ly} = \int_0^1 \kappa_{yl}\phi_i\phi_j\delta(\xi-\xi_S)\,d\xi, \qquad \text{(B.14)}$$

$$\kappa_{ij}^{lz} = \int_0^1 \kappa_{zl}\psi_i\psi_j\delta(\xi-\xi_S)\,d\xi, \qquad \text{(B.15)}$$

$$\kappa_{ijkl}^{nly} = \int_0^1\left(\kappa_{ynl}\phi_i\phi_j\phi_k\phi_l\delta(\xi-\xi_s) + \kappa_x \mathrm{K}_{ijkl}\right)d\xi, \qquad \text{(B.16)}$$

$$\kappa_{ijkl}^{yzz} = \int_0^1\left(\kappa_{yz}\phi_i\phi_j\psi_k\psi_l\delta(\xi-\xi_s) + \kappa_x \mathrm{K}_{ijkl}\right)d\xi, \qquad \text{(B.17)}$$

$$\kappa_{ijkl}^{nlz} = \int_0^1\left(\kappa_{znl}\psi_i\psi_j\psi_k\psi_l\delta(\xi-\xi_s) + \kappa_x \mathrm{K}_{ijkl}\right)d\xi \qquad \text{(B.18)}$$

$$\kappa_{ijkl}^{zyy} = \int_0^1\left(\kappa_{yz}\psi_i\psi_j\phi_k\phi_l\delta(\xi-\xi_s) + \kappa_x \mathrm{K}_{ijkl}\right)d\xi, \qquad \text{(B.19)}$$

$$\mathrm{K}_{ijkl} = \phi_i\phi_j'\delta(\xi-\xi_s)\int_0^\xi \phi_k'\phi_l'\,d\xi$$
$$-\mu(0\to\xi_s)\phi_i\phi_j''\int_0^{\xi_s}\phi_j'\phi_j'\,d\xi, \qquad \text{(B.20)}$$

$$\int_0^1 \mathrm{K}_{ijkl}\,d\xi$$
$$= \int_0^1\left[\phi_i\phi_j'\delta(\xi-\xi_s)\int_0^\xi \phi_k'\phi_l'\,d\xi - \mu(0\to\xi_s)\phi_i\phi_j''\int_0^{\xi_s}\phi_j'\phi_j'\,d\xi\right]d\xi$$
$$= \left[\phi_i\phi_j'\right]_{\xi=\xi_s}\int_0^{\xi_s}\phi_k'\phi_l'\,d\xi - \int_0^{\xi_s}\phi_i\phi_j''\int_0^{\xi_s}\phi_j'\phi_j'\,d\xi d\xi. \qquad \text{(B.21)}$$